Terahertz-Laser Control of Large Amplitude Vibrational Motion in the Sub-One-Cycle Pulse Limit

N. Došlić*

Department of Physical Chemistry, R. Bošković Institute, Bijenička 54, 10000 Zagreb, Croatia

Received: July 11, 2006; In Final Form: August 28, 2006

We investigate the control of state-selective population transfer in the THz spectral range generated by sub-one-cycle pulse excitation. To this end we developed a zero-net-force modification of the optimal control algorithm which allows us to extend the algorithm into the ultrashort pulse domain. By combining the analysis of the control landscapes and that of optimal control theory, we were able to formulate a general mechanism suitable for laser control by ultrashort pulses. The strategy consists of a superposition of two π-pulses with carrier envelope phases of $\phi = \pi/2$. The first pulse is effectively in resonance with the targeted transition, while the second one, fired at around the minimum of the first pulse second lobe, removes leaking to the dipole-coupled background state. To compensate for the pulses ultrashort duration, the carrier frequencies of both pulses are red-shifted from the spectroscopic resonance.

I. Introduction

Few-cycle laser pulses are powerful tools for studying fundamental aspects of light−matter interaction.[1−4] The reason for their effectiveness lies in the fact that the dynamics of the material system is highly sensitive to details of the subcycle laser pulse shape. Traditional many-cycle pulses are parametrized as products of their envelope function and the carrier wave frequency. However, to fully characterize the shape of the electric field of a few-cycle laser pulse, one needs to specify also the carrier-envelope (CE) or absolute phase of the pulse. The latter, defined as the relative phase that the maximum of the carrier wave has with respect to the pulse envelope, is the crucial parameter to be stabilized in order to gain control over the system dynamics.[5]

In the last couple of years fast progress in laser technology has made it possible to determine the value of the absolute phase[6−8] and to achieve active control over it,[9] hence paving the way to applications in molecular dynamics.

Yet, rather few theoretical[10] and virtually no experimental studies[11,12] have addressed molecular dynamics in the few-cycle pulse regime. State of the art quantum simulations have shown that phase matching combinations of few-cycle infrared (IR) and ultraviolet (UV) pulses are capable of breaking molecular symmetry and achieving spatial separation of competing products of photodissociation.[13,14] Well-timed IR+UV combinations have been used to excite large amplitude torsional motion on the ground PES and subsequently to induce unidirectional intramolecular rotation on the excited PES.[15]

Turning to few-cycle IR pulses, we have analyzed laser-driven tunneling in model one- and two-dimensional systems and proposed to control the motion by half-cycle pulses as alternatives to the static electromagnetic field.[16,17] Numerical simulations indicated a transition from phase-insensitive to phase-sensitive dynamics as the laser carrier frequency swept away from resonance.[18−20] However, an analytical understanding of the onset of carrier envelope phase dependent dynamics has been achieved only recently.[21] By solving the time dependent Schrödinger equation in the interaction representation via time ordered exponentials, Uiberacker and Jakubetz were capable of treating two limiting situations.[21] One of them is the case when the pulse carrier frequency is much larger than the system transition frequency, and the population dynamics exhibited no phase dependence. The opposite limit, when the carrier frequency is much smaller than the system frequency, displayed dependence of the final state population on the sign of the electric field.

In this paper we consider the case when the pulse carrier frequency approaches the system transition frequency. In ref 21 this intermediate case was treated as a combination of terms arising from the two limiting cases. Jirauschek et al.[22] found that at resonance the phase-dependence of the population dynamics emerges only in the nonlinear field regime, when the pulse power spectrum $E(\omega) = \int_{-\infty}^{\infty} E(t)e^{i\omega t}$ acquires CE phase dependence. We have been also concerned with the population inversion generated by sub-one-cycle pulse excitation[23,24] and primarily with changes occurring in the Rabi-type dynamics. Specifically, we found a shortening of the Rabi inversion period and proved that complete inversion is unobtainable under resonant, ultrashort pulse condition.[24] In the present contribution we extend these findings to the control of large amplitude motion with the goal of developing robust strategies for frequency-driven population inversion in the terahertz spectral range. In laser control the rule of the game is to make the transition as fast as possible while retaining the maximum selectivity. In view of this, sub-one-cycle THz laser pulses became natural tools for laser control of large amplitude vibrations such as the intramolecular H-transfer motion in acetylacetone treated in this paper.

The rest of the paper is organized as follows: Section II describes the interaction of material system with an ultrashort laser pulse and extends optimal control theory into the sub-one-cycle pulse domain. Section III summarizes the characteristics of the model system. Results are presented in section IV. First the landscape of the control area is investigated in section

* Corresponding author e-mail: nadja.doslic@irb.hr.

10.1021/jp064363i CCC: $33.50
Published on Web 10/25/2006

IVA, and then the dynamics underlying optimal control theory is analyzed in section IVB. The final section contains the conclusion.

II. Theoretical and Computational Background

Before proceeding with the implementation of optimal control theory in the subcycle pulse limit it is useful to review some technical issues of laser−matter interaction in the ultrashort regime. In the length gauge the time dependent Schroedinger equation describing the dynamics of a system with dipole moment $\mu(\vec{r})$ interacting with the electromagnetic field reads

$$i\hbar \frac{\partial}{\partial t}\Psi(\vec{r}, t) = \left[H_0(\vec{r}) + \frac{\mu(\vec{r})}{c}\frac{\partial A(t)}{\partial t}\right]\Psi(\vec{r}, t) \qquad (1)$$

where $H_0(\mathbf{r})$ is the unperturbed Hamiltonian of the system, and $A(t)$ is the vector potential of the form

$$A(t) = -\frac{F_0 c}{\omega} m(t)\sin(\omega t + \phi) \qquad (2)$$

The electric field $E(t)$ is then given by

$$E(t) = -\frac{1}{c}\frac{\mathrm{d}A(t)}{\mathrm{d}t} = F_0 m(t)\cos(\omega t + \phi) + \frac{F_0}{\omega}\frac{\mathrm{d}m(t)}{\mathrm{d}t}\sin(\omega t + \phi) \qquad (3)$$

The first term in eq 3 corresponds to the 'traditional' radiation pulse having a bell-shaped envelope function $m(t)$, a monochromatic carrier wave of frequency ω, and a carrier envelope phase ϕ. For such a radiation pulse in a two-level system characterized by a dipole matrix element μ_{12}, a π-pulse defined as

$$\frac{F_0 \mu_{12}}{2}\int_0^T m(t)\mathrm{d}t = \pi \qquad (4)$$

leads to complete population inversion. The second term, containing the time derivative of the pulse envelope, is negligible in the many-cycle pulse case where the slowly varying envelope approximation is valid, but gains in importance, and actually becomes comparable to the first term in the sub-one-cycle pulse limit.

Following Brabec and Krausz[1] we assumed a time-dependent envelope function $m(t)$, centered at $t = 0$ of the form

$$m(t) = sech\left(\frac{t}{\alpha}\right) \qquad (5)$$

where $\alpha_{1/2} = \alpha \ln(2 + \sqrt{3})$ is the half width of the pulse at half-maximum (HWHM). Experimentally $2\alpha_{1/2}$ (FWHM) is referred to as the pulse duration, but in numerical simulations it is more convenient to define the pulse duration as the interval outside which the electric field is effectively zero. Specifically we have assumed $T = 2s_0\alpha$ with $s_0 = 6.5$. It is important to notice that the envelope derivative term, which arises because of the finite pulse duration, ensures the fulfillment of the zero-net-force condition[1,25,26]

$$\int_{-\infty}^{\infty} E(t)\mathrm{d}t = 0 \qquad (6)$$

or, in other words, it guarantees that the electric field given in eq 3 is a solution of the Maxwell equations in the propagation region.

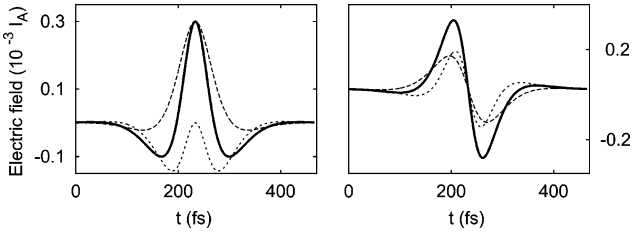

Figure 1. 0.33-cycle pulses with CE phases $\phi = 0$ (left) and $\phi = \pi/2$ (right). The total electric field of the pulse (bold line) is compared with its two components: the 'traditional' pulse consisting of an envelope and cosine carrier field (dashed line) and the time derivative of the pulse envelope with a sine carrier field (dotted line).

An ultrafast pulse can be characterized by the number of carrier wave oscillation contained within the pulse width measured at half the maximum[6,18]

$$2\alpha_{1/2} = n_c T = n_c \frac{2\pi}{\omega} \qquad (7)$$

In Figure 1 we display the time variation of the total electric field of two ultrashort, $n_c = 0.33$ pulses with CE $\phi = 0$ (cosine-pulse) and $\phi = \pi$ (sine-pulse) together with the two field components specified in eq 3. By comparing the total field form with its 'traditional' form (dashed line) two effects can be seen: First, in the ultrashort limit, $\phi = \pi/2, 3\pi/2, 5\pi/2...$ pulses acquire higher peak field strengths and, in general, have larger fluence than corresponding $\phi = 0, \pi, 2\pi...$ pulses

$$F_E = \int_{-\infty}^{\infty} E(t)^2\mathrm{d}t = {F_0}^2\alpha\left(1 + \frac{1}{3m_c\pi^2}\right) - \frac{{F_0}^2\alpha(1 + m_c\pi^2)\cos(2\phi)\mathrm{cosech}(m_c\pi^2)}{3m_c} \qquad (8)$$

where $m_c = n_c/\ln(2 + \sqrt{3})$. Second, the inclusion of the envelope function derivative term results in an effective increase of the pulse frequency.[24] This can be readily seen by comparing the shape of the electric field around the pulse peaks. The effect can be quantified by making use of eq 7 and by equating the electric field of an ultrashort pulse at lower frequency $\omega - \delta$ to that of a 'traditional' pulse (first term in eq 3) at frequency ω

$$F_0\,\mathrm{sech}\left(\frac{(\omega - \delta)t}{m_c\pi}\right)\left(\cos((\omega - \delta)t) - \frac{\sin((\omega - \delta)t)}{m_c\pi}\tanh\left(\frac{(\omega - \delta)t}{m_c\pi}\right)\right) = F_0\,\mathrm{sech}\left(\frac{\omega t}{m_c\pi}\right)\cos(\omega t) \qquad (9)$$

The frequency shift is then easily obtained by expanding the equation around $t = 0$ and solving for δ

$$\delta = \omega\left(1 - \frac{1 + {m_c}^2\pi^2}{\sqrt{3 + 4{m_c}^2\pi^2 + {m_c}^4\pi^4}}\right) \qquad (10)$$

As it will be apparent shortly, the effective increase of the pulse frequency is one of the key features of laser control in the sub-one-cycle pulse domain.

To implement optimal control theory[27−29] in the ultrashort pulse limit, the zero-net-force condition (eq 6) has to be enforced. For this purpose let us introduce the penalty factor λ_0 which weighs the magnitude of the DC component. The objective functional to be maximized is then

$$J_{fi} = |\langle\psi_i(T)|\phi_f(T)\rangle|^2 - \alpha_0\int_0^T \frac{|\epsilon(t)|^2}{s(t)}\,dt - \lambda_0\int_0^T \epsilon(t)dt \quad (11)$$

$$- 2Re\left[\langle\psi_i(T)|\phi_f\ (T)\rangle\int_0^T \langle\psi_f(t)\left|\frac{\partial}{\partial t} + i[H_0 - \mu\epsilon(t)]|\psi_i(t)\rangle dt\right]\right. \quad (12)$$

where $\psi_i(t)$ is the initial wave function, $\epsilon(t)$ is the optimal driving field, and $\psi_f(t)$ is the Lagrange multiplier ensuring the satisfaction of the Schrödinger equation. The system dependent parameter α_0 weighs the laser fluence, and the shape function $s(t)$ ensures a smooth switch on/off behavior of the field. The condition for obtaining the extremum of the functional J_{fi} leads to a standard set of differential equations for the wave function and the Lagrange multiplier, while the optimal field is given by

$$\epsilon(t) = -\frac{s(t)}{\alpha_0}[Im\langle\psi_i(t)|\phi_f\ (t)\rangle\langle\psi_f\ (t)|\mu|\psi_i(t)\rangle + \lambda_0] \quad (13)$$

In the derivation of eq 13 the terms proportional to $(\delta\epsilon(t))^2$ have been neglected. Hence memory effects, useful when dealing with complex target states in the continuum, have not been taken into account.[30]

Alternative strategies to deal with laser control in the few-cycle pulse limit can be envisaged. For example, one may start from the time dependent Schrödinger equation in the velocity gauge and derive a system of equations in terms of the vector potential. However, when facing bound-state problems the present formulation appears to be more convenient.

II.1. Model System. The present work is concerned with laser control of large amplitude nuclear motion in a multidimensional quantum system. As a model system we have selected acetylacetone (ACAC), a prototype molecule for symmetric, intramolecular hydrogen transfer. The potential energy and dipole moment surface[31] are constructed using three large amplitude internal coordinates q given by

$$q_1 = r_1 + r_2$$

$$q_2 = r_2 - r_2$$

$$q_3 = \theta \quad (14)$$

where r_1 is the distance from the hydrogen to the donor oxygen atom, r_2 is the distance from the hydrogen to the acceptor oxygen atom, and θ is the OHO angle. In terms of (q_1, q_2, q_3) the molecular Hamiltonian reads

$$\hat{H}_0 = -\frac{\hbar^2}{2}\sum_{r=1}^{M}\sum_{s=1}^{M}\frac{\partial}{\partial q_r}\left[G^{rs}\frac{\partial}{\partial q_s}\right] + V(q_1, q_2, q_3) \quad (15)$$

where the kinetic energy matrix elements G^{rs} are calculated as

$$G^{rs} = \sum_{i=1}^{3N}\frac{1}{m_i}\frac{\partial q_r}{\partial x_i}\frac{\partial q_s}{\partial x_i} \quad (16)$$

and $\{x_i\} \equiv \boldsymbol{x}$ is the corresponding set of 3N Cartesian coordinates. While the computational details of the eigenspectrum are given in ref 31, we mention here that the lowest eigenvalue of the system at 5.64 kcal mol^{-1} is energetically above the C_{2v} transition structure at 2.70 kcal mol^{-1}, indicating that tunneling plays no role in the H-transfer reaction in ACAC. However, the double well symmetry of the PES induces splitting of all vibrational levels. In our three dimensional model the ground state splitting of ACAC is $\omega(0^+ \leftarrow 0^-) = 3.5$ THz. The two lowest O−O stretching doublets exhibit larger splittings of $\omega(1^+ \leftarrow 1^-) = 5.5$ THz and $\omega(2^+ \leftarrow 2^-) = 6.0$ THz, while the energy differences between the three lowest doublets are $\omega(0^- \leftarrow 1^+) = 6.7$ THz and $\omega(1^- \leftarrow 2^+) = 5.8$ THz. A schematic representation of the lowest energy levels is given in Figure 2 together with the more simple notation indicated on the left of the scheme.

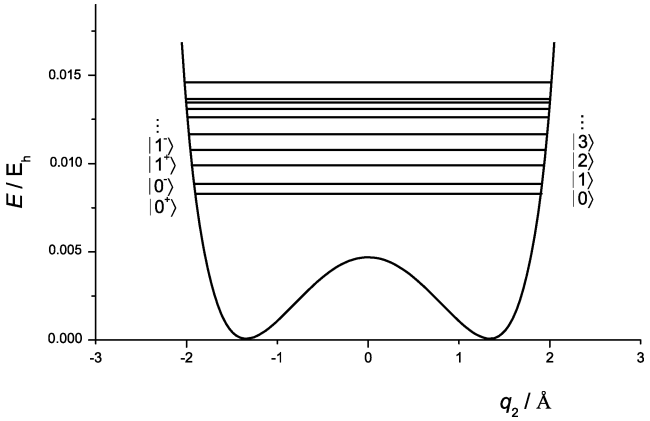

Figure 2. Schematic 1D cut through the 3D PES of ACAC. The eigenvalues of the lowest 10 states of the 3D surface are indicated by horizontal bars. The lowest eigenvalue $|0\rangle$ is above the C_{2v} structure at 2.7 kcal mol^{-1}.

In the following a population inversion between the two ground-state levels of ACAC is sought. Frequency-wise the ground-state transition appears well separated from the adjacent $|2\rangle \leftarrow |1\rangle$ transition at 6.7 THz. However, the inspection of the dipole moment matrix elements reveals strong coupling between adjacent doublets that may influence the selectivity of the vibrational transition.

III. Results and Discussion

III.1. Analysis of State-Selective Population Transfer. According to eq 7 a one-cycle pulse with carrier frequency $\omega = 3.5$ THz has a duration of $t_p = 1869$ fs. On this time scale intramolecular vibrational energy redistribution is expected to take place in ACAC, since the H-transfer mode is notoriously strongly coupled to low-frequency modes of the molecular framework.[32] Hence, we first investigate the laser control area by third-of-cycle pulses. The final population of the $|1\rangle$ state obtained by scanning the amplitude and carrier wave frequency of the electric field is shown in Figure 3. The images have been obtained by fixing the absolute phase of the laser pulse to $\phi = 0$ and $\phi = \pi$ on the left panel and to $\phi = \pi/2$ and $\phi = 3\pi/2$ on the right one. To allow for vibrational wave packet formation at high field strengths, eq 1 has been solved in the basis of the lower 50 eigenstates of the system. Altogether 7500 simulations have been performed for each of the four CE phases in the range $0 \le E_0 \le 0.003$ I_A and $0.6 \le \omega \le 4.8$ THz. As can be inferred from Figure 3, however, the strong phase sensitivity characteristic for wave packet driven reactions has not been found in ACAC. On the contrary, the control landscape can be quite well rationalized in terms of a vibrational progression in a N-level system.

Two control areas can be readily identified. In the first one, spanned by $1.5 < \omega < 3.0$ THz and $0.00025 < E_0 < 0.00060$ I_A, a control yield close to 90% is achieved. For $\phi = 0$ and $\phi = \pi$ peak populations of $P_1 = 0.89$ are obtained at $\omega = 2.1$ THz and $E_0 = 0.00042$. The corresponding population dynamics

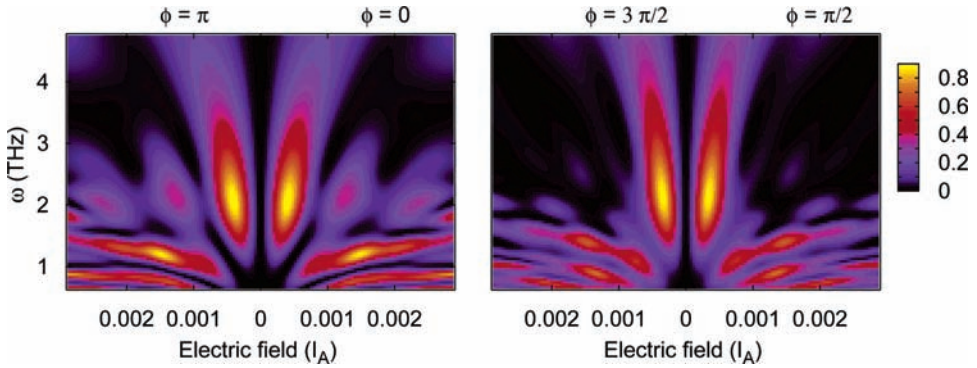

Figure 3. Target state population at the end of a $n_c = 0.33$ pulse excitation. The variation of the final population is shown as a function of the electric field strength and carrier frequency. The CE phases are $\phi = \pi$, 0 (left) and $\phi = 3\pi/2$, $\pi/2$ (right).

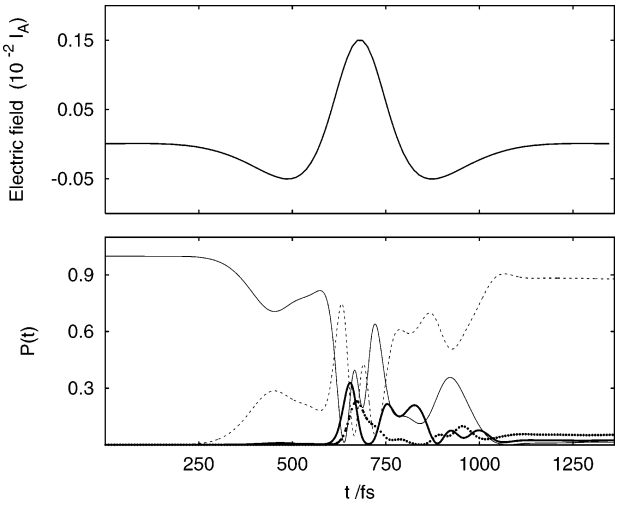

Figure 4. Top: electric field of an $n_c = 0.33$ pulse with sech-type envelope, $\omega = 1.2$ THz, $E_0 = 0.00015$ I_A, and $\phi = 0$. Bottom: time-resolved population of the lowest four states. P_0 (solid, thin), P_1 (dotted, thin), P_2 (solid, bold), and P_3 (dotted, bold).

corresponds to a Rabi-type transition between states $|0\rangle$ and $|1\rangle$ with population leaking to $|2\rangle$. As explained in section II, because of the rapid onset of the field a 0.33-cycle pulse acquires an effective frequency that is higher than its carrier wave frequency. Hence a 0.33-cycle pulse with carrier frequency $\omega = \omega_{01} - \delta$ is effectively in resonance with the $|1\rangle \leftarrow |0\rangle$ transition at ω_{01}. According to eq 10, the frequency shift amounts to $\delta = 1.15$ THz. The generalized π-pulse condition is, therefore, satisfied by a pulse with frequency of $\omega = 2.3$ THz that turns out to be in good agreement with the obtained numerical value of $\omega = 2.1$ THz. We note, however, that the frequency of the maximum efficiency pulse has been further shifted to the red because of the target state being the middle state in a *I*-type three-level system.[33]

Comparing the behavior of extreme cosine ($\phi = 0$, π) and sine ($\phi = \pi/2$, $3\pi/2$) pulses one notices that sine-pulses achieve maximum population transfer at lower field strength. Specifically, the highest control yield is obtained at $E_0 = -0.00034$ I_A and $\omega = 72.2$. The effect is a consequence of the CE phase dependence of the pulse fluence given in eq 8.

Let us now investigate the dynamics in the second control area spanned by $0.6 < \omega < 1.5$ THz and $0.001 < E_0 < 0.003$ I_A. Immediately, a high sensitivity of the target state population with respect to the pulse parameters is observed. Efficient control is restricted to narrow parameters islands. Figure 4 displays the population dynamics of the lowest five vibrational states driven by a top-efficiency pulse with parameters $\omega = 1.2$ THz, $E_0 = -0.00151$ I_A, and $\phi = 0$. Although at the end of the pulse the population of the target state reaches $P_1 = 0.87$, during the interaction with the laser pulses high lying vibrational states are populated with peaks above $P_2 = 0.3$. This larger number of states involved in the control gives rise to a pronounced phase sensitivity, as can be seen by comparing the respective areas on the left and right panel. Also, in this regime a switch from phase insensitive frequency-driven transitions to phase sensitive dipole-driven transitions is expected to occur. However, because of the imposed zero-net-force condition and the asymmetry of the *x*-component of the ACAC dipole moment the final populations are symmetric with respect to changes of the CE phase by π. These strong field control areas are clearly less suitable for laser control, but their analysis may turn out useful in experimental feedback control. Specifically, a control mechanism involving high lying vibrational states would be characterized by the variation of the feedback field with respect to the initial guess, with the instability of the control yield with respect to small variation in field parameters and with the requirement for high field strengths.

By fixing the number of carrier wave oscillations to $n_c = 0.33$ we have allowed changes in the pulse duration. For example, a pulse with carrier wave frequency $\omega = 1.2$ THz has a duration of 1355 fs, while a pulse with frequency $\omega = 4.8$ THz has a duration of only 338 fs. However, in a typical optimal control simulation the pulse duration is fixed, whereas no restriction on the number of oscillations of the carrier is imposed. In Figure 5 the pulse duration has been fixed at 750 fs, and the variation of the target state population with respect to the carrier frequency and intensity for four CE phases is shown. The duration of the pulses corresponds to that of a top-efficiency $n_c = 0.33$ pulse with frequency $\omega = 72.2$ (see Figure 3). To facilitate comparison between different pulses the width of the time-dependent envelope function was kept constant. With that restriction, low-frequency pulses with $\omega < 1.2$ THz do not meet the numerical threshold of the zero net-force condition (eq 6) and were not displayed. Clearly, the position and contrast of the peaks depend on the absolute phase. The cosine-pulse ($\phi = 0,\pi$) driven dynamics, shown on the left, present a broad, frequency insensitive area of high yield control. Because of the coincidence between the envelope and carrier wave maxima the shape of the pulse is governed by the envelope function and is less sensitive on the carrier wave frequency. On the contrary, the carrier frequency is a more important control parameter for sine-type pulses. Since the $|1\rangle \leftarrow |0\rangle$ population transfer efficiency is dependent on the carrier wave frequency, two-lobe pulses appear more suitable for laser control purposes. Namely, they can be more easily modified and possibly improved by frequency chirping.

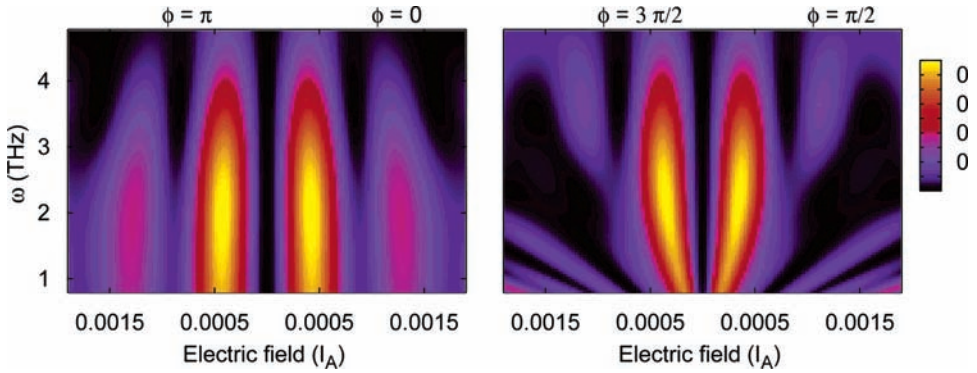

Figure 5. Target state population at the end of a 750 fs pulse excitation. The variation of the final population is shown as a function of the electric field strength and carrier frequency. The CE phases are $\phi = \pi$, 0 (left) and $\phi = 3\pi/2$, $\pi/2$ (right).

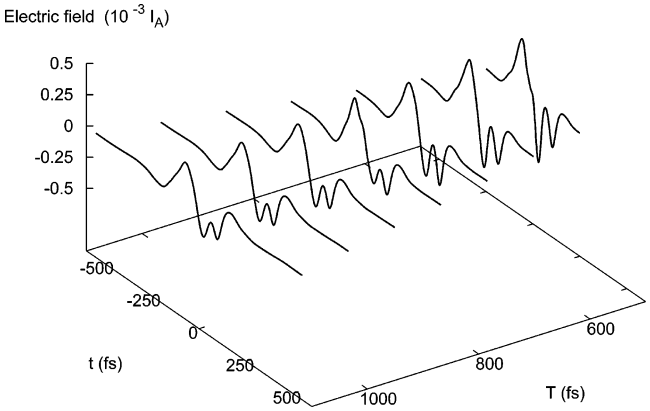

Figure 6. Near-invariance of the optimal control theory pulses. Time variation of the electric field for several pulses with duration $450 \leq T \leq 1050$ fs.

III.2. Optimal Control Theory Results. In the previous section quite large population transfer yields for the ground-state inversion in ACAC have been achieved by using simple pulses. Therefore, the improvement via optimal control is expected to occur by subtle changes of the simple Rabi-type dynamics. Accordingly, in our optimal control simulations the penalty factor α was kept quite hight (100−400) in order to avoid multiple population transfers between the initial and target state.

Figure 6 shows a number of highly efficient ($P_1 > 0.96$) pulses in the range between $450 \leq t_p \leq 1100$ fs obtained by using our zero-net force variant of optimal control theory. The threshold for the DC field component was set to 0.1. A striking similarity among the pulses is readily observed. All pulses are characterized by the same absolute phase of $\phi = \pi/2$ and by an increase of the frequency in the second lobe of the pulse. Actually, the pulse appears as a superposition of two pulses: a longer pulse with CE phase $\phi = \pi/2$, and a monochromatic carrier, and a much shorter pulse centered at around the minimum of the second lobe.

The analysis of the population dynamics helps in deciphering the optimal control mechanism. Figure 7 (top) displays three pulses with duration $t_{pulse} = 750$ fs and CE phase $\phi = \pi/2$. The corresponding population evolution curves for the target state $|1\rangle$ and for the strongly coupled state $|2\rangle$ are shown on the lower panel. The simple pulse (solid, thin) with parameters $n_c = 0.33$, $\omega = 2.2$ THz, $E_0 = 0.00034$ achieves a target state population of $P_1 = 0.89$, while the remaining population is mostly located in $|2\rangle$ with $P_2 = 0.09$. Actually, this simple pulse is the most effective generalized π-pulse lying in the middle of the Rabi-type control area shown in Figure 3. The optimal control pulse (solid, bold) achieves a target state population of $P_1 = 0.98$.

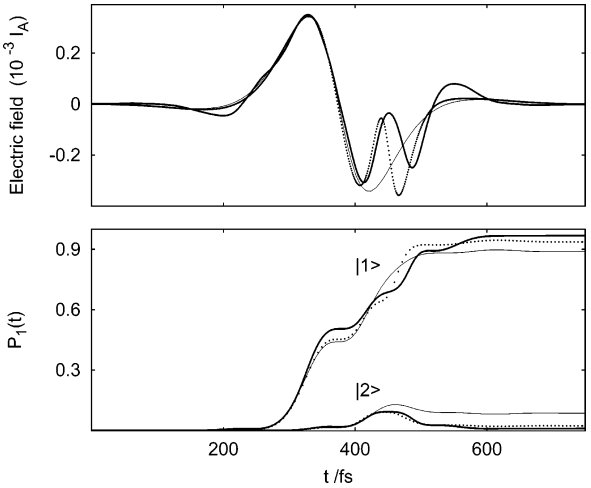

Figure 7. Top: Superposition of three control pulses with sech-type envelope and duration of 750 fs. Monochromatic $n_c = 0.33$ pulse with $\omega = 2.2$ THz, $E_0 = 0.00034$ I_A (solid, thin). Optimal control theory pulse (solid, bold). Compound pulse (dotted) obtained as a superposition of two pulses with parameters: $n_c^{(1)} = 0.33$, $\omega^{(1)} = 2.3$ THz, $E_0^{(1)} = 0.00037$ I_A, $n_c^{(2)} = 0.33$, $\omega^{(2)} = 4.5$ THz, $E_0^{(2)} = 0.00025$ I_A. The center of the second pulse is at 450 fs. Bottom: the corresponding time-resolved populations of the target state $|1\rangle$ and the background state $|2\rangle$.

Although both pulses have comparable P_2 populations at 450 fs, at the end of the optimal control pulse the population of $|2\rangle$ is successfully driven back to the target state. The effect is obviously caused by the peculiar shape of the second lobe. To investigate this possibility we constructed the following compound pulse. The first third-of-cycle pulse with $\omega = 2.3$ THz and $E_0 = 0.00037$ I_A matches well the first lobe of the optimal control pulse (see Figure 7). At 450 fs, i.e., at the time when the background-state reaches its maximum, we place the second $n_c = 0.33$ pulse with $\phi = \pi/2$ and $\omega_2 = 4.5$ THz. The carrier frequency of the second pulse is effectively in resonance with the $|2\rangle \leftarrow |1\rangle$ transition at 6.7 THz, but the frequency has been corrected to compensate for its ultrashort duration according to eq 10. The corresponding pulse and population dynamics are shown by dotted lines.

Clearly, the two pulses superposition is very efficient and triggers a population dynamics similar to the one obtained by the OCT pulse. The role of the second pulse, which on the fly corrects for the leaking to $|2\rangle$, is essential for obtaining a large control yield. It is worth noticing that the electric field strength of the second pulse was the only parameter optimized numerically.

Finally, let us make a detour into the multicycle pulse dynamics and discuss some strategies for laser control of state-

selective population transfer. Recently, Etinski et al.[34] have proposed a control strategy in which a superposition of pulses successfully removes leaking to the strongly coupled background state. Apart from the main resonant π pulse, an additional pulse with a numerically optimized envelope function displaying two maxima, and frequency close to the energy difference between the target and intruder state, acts on the system. The timing of the auxiliary pulse coincides approximately with the onset of the background state population. Details of the underlying mechanism are not completely clear because of the multicycle nature of the employed pulses. However, it turns out that the approach of Etinski et al.[34] is a variant of the counterdiabatic strategy of Demirplak and Rice[35] based solely on the analysis of the background-state population dynamics. The presented optimal control results and the two π-pulses mechanism appear as counterparts of these strategies in the sub-one-cycle pulse regime.

IV. Conclusion

This work investigates strategies for laser control in the terahertz spectral range. It deals with the large amplitude H-transfer motion in ACAC, but it is our belief that the results are general and applicable to any system whose dynamics calls for control in the sub-one-cycle pulse domain. In particular, the zero-net-force condition imposed on the electric filed, i.e., the definition of the electric field via its vector potential, provides a reliable framework for analyzing laser-matter interaction in the ultrashort pulse limit. In addition, we developed a zero-net-force modification of the optimal control theory algorithm which allows us to effectively control the dynamics in that limit.

The presented results demonstrate that sub-one-cycle pulses can achieve high control yields in state-selective population transfer. This conclusion is valid in both the weak field limit where Rabi-type population transfer occurs and in the strong field limit. The latter mechanism involves multiple population transfer between the initial and the target state as well as population of high-lying vibrational states. It is therefore restricted to narrow areas of laser field parameters. This sensitivity of laser control in the strong field regime is reflected in the optimal control theory results. Namely, the optimal control theory algorithm allows large changes of the electric field from one iteration to another and preferentially converges in the large area of pulse parameters approximately fulfilling the generalized π-pulse condition. Consequently, the laser pulses obtained in OCT simulations are effective, robust, and applicable in a time-window of more than 500 fs.

Moreover, by combining the information contained in the analysis of the control landscape and that revealed by optimal control, we were able to decipher a more general laser control mechanism acting in the ultrashort pulse regime. The strategy consists of superimposing two π-pulses with CE phases of $\phi = \pi/2$. The first one is resonant with the targeted transition, while the second one, fired at around the minimum of the second lobe, removes leaking to the most strongly coupled intruder state. Of course, the carrier frequency of both pulses must be red-shifted from resonance to compensate for their ultrashort duration.

Acknowledgment. The author thanks W. Jakubetz (Vienna), J. Manz (Berlin), and D. B. Milošević (Sarajevo) for assistance and stimulating discussions. This work has been supported by the Croatian Ministry of Science and Education under project No. 0098033 and the Humboldt Foundation.

References and Notes

(1) Brabec, T.; Krausz, F. *Rev. Mod. Phys.* **2000**, *72*, 545.
(2) Drescher, M.; Hentschel, M.; Kienberger, R.; Tempea, G.; Spielmann, C.; Reider, G. A.; Corkum, P. B.; Krausz, F. *Science* **2001**, *291*, 1923.
(3) Milošević, D. B.; Paulus, G. G.; Bauer, D.; Becker, W. *J. Phys. B* **2006**, *39*, 203.
(4) Niikura, H.; Villeneuve, D. M.; Corkum, P. B. *Phys. Rev. A* **2006**, *73*, 021402(R).
(5) Paulus, G. G.; Grasbon, F.; Walther, H.; Villoresi, P.; Nisoli, M.; Stagira, S.; Priori, E.; De Silvestiri, S. *Nature (London)* **2001**, *414*, 182.
(6) Paulus, G. G.; Lindner, F.; Walther, H.; Baltuška, A.; Gouuliel-makis, E.; Lezius, M.; Krausz, F. *Phys. Rev. Lett.* **2003**, *91*, 253004.
(7) Fortier, T. M.; Roos, P. A.; Jones, D. J.; Cundiff, S. T.; Bhat, R. D. R.; Sipe, J. E. *Phys. Rev. Lett.* **2004**, *92*, 147403.
(8) Mücke, O. D.; Tritschler, T.; Wegener, M.; Morgner, U.; Kärtner, F. X.; Khirtova, G.; Gibbs, H. M. *Opt. Lett.* **2004**, *29*, 2160.
(9) Baltuška, A.; Udem, Th.; Uiberacker, M.; Hentschel, M.; Goulielmakis, E.; Gohle, Ch.; Holzwarth, R.; Yakovlew, V. S.; Scrinzi, A.; Hänsch, T. W.; Krausz, F. *Nature* **2003**, *421*, 611.
(10) Kalugin, N. G.; Rostovtsev, Y. V.; Scully, M. O. *eprint arXiv: quant-ph/0602142*, 2006.
(11) Kawashima, H.; Wefers, M. M.; Nelson, K. A. *Annu. Rev. Phys. Chem.* **1995**, *46*, 627.
(12) Ferguson, B.; Zhang, X.-C. *Nat. Mater.* **2002**, *1*, 26.
(13) Elghobashi, N.; Krause, P.; Manz, J.; Oppel, M. *Phys. Chem. Chem. Phys.* **2003**, *5*, 4806.
(14) Elghobashi, N.; González, L.; Manz, J. *J. Chem. Phys.* **2004**, *120*, 8002.
(15) Fujimura, Y.; González, L.; Kröner, D.; Manz, J.; Mehdaoui, I.; Schmidt, B. *Chem. Phys. Lett.* **2004**, *386*, 248.
(16) Došlić, N.; Kühn, O.; Manz, J.; Sundermann, K. *J. Phys. Chem.* **1998**, *102*, 9645.
(17) Došlić, N.; Sundermann, K.; González, L.; Mó, O.; Giraud-Girard, J.; Kühn, O. *Phys. Chem. Chem. Phys.* **1999**, *1*, 1249.
(18) Uiberacker, C.; Jakubetz, W. *J. Chem. Phys.* **2004**, *120*, 11532.
(19) Uiberacker, C.; Jakubetz, W. *J. Chem. Phys.* **2004**, *120*, 11540.
(20) Tatić, I.; Došlić, N. *Croat. Chem. Acta* **2004**, *77*, 83.
(21) Uiberacker, C.; Jakubetz, W. *J. Chem. Phys.* **2006**, in press.
(22) Jirauschek, Ch.; Duan, L.; Mücke, O. D.; Kärtner, F. X.; Wegener, M.; Morgner, U. *J. Opt. Soc. Am. B* **2005**, *22*, 2065.
(23) Došlić, N.; Kühn, O. *Chem. Phys.* **2000**, *255*, 247.
(24) Došlić, N. *Phys. Rev. A* **2006**, *74*, 013402.
(25) Bandrauk, A. D.; Shon, N. H. *Phys. Rev. A* **2002**, *66*, 031401.
(26) Rauch, J.; Mourou, G. *Proc. Am. Math. Soc.* **2005**, in press.
(27) Zhu, W.; Botina, J.; Rabitz, H. *J. Chem. Phys.* **1998**, *108*, 1953.
(28) Tannor, D.; Rice, S. A. *J. Chem. Phys.* **1985**, *83*, 5013.
(29) Sundermann, K. de Vivie-Riedle, R. *J. Chem. Phys.* **1999**, *110*, 1896.
(30) Geppert, D.; de Vivie-Riedle, R. *Chem. Phys. Lett.* **2005**, *404*, 289.
(31) Matanivić, I.; Došlić, N. *J. Phys. Chem. A* **2005**, *109*, 4185.
(32) May, V.; Kühn, O. *Charge and Energy Transfer Dynamics in Molecular Systems*; Wiley-VCH: Berlin, 2000.
(33) Bonacci, D.; Bosanac, S. D.; Došlić, N. *Phys. Rev. A* **2004**, *70*, 043413.
(34) Etinski, M.; Uiberacker, C.; Jakubetz, W. *J. Chem. Phys.* **2006**, *124*, 124110.
(35) Demirplak, M.; Rice, S. A. *J. Phys. Chem.* **2003**, *107*, 9937.